

MPT: Mesh Pre-Training with Transformers for Human Pose and Mesh Reconstruction

Kevin Lin, Chung-Ching Lin, Lin Liang, Zicheng Liu, Lijuan Wang
Microsoft

{keli, chungching.lin, lliang, zliu, lijuanw}@microsoft.com

Abstract

We present *Mesh Pre-Training (MPT)*, a new pre-training framework that leverages 3D mesh data such as MoCap data for human pose and mesh reconstruction from a single image. Existing work in 3D pose and mesh reconstruction typically requires image-mesh pairs as the training data, but the acquisition of 2D-to-3D annotations is difficult. In this paper, we explore how to leverage 3D mesh data such as MoCap data, that does not have RGB images, for pre-training. The key idea is that even though 3D mesh data cannot be used for end-to-end training due to a lack of the corresponding RGB images, it can be used to pre-train the mesh regression transformer subnetwork. We observe that such pre-training not only improves the accuracy of mesh reconstruction from a single image, but also enables zero-shot capability. We conduct mesh pre-training using 2 million meshes. Experimental results show that MPT advances the state-of-the-art results on *Human3.6M* and *3DPW* datasets. We also show that MPT enables transformer models to have zero-shot capability of human mesh reconstruction from real images. In addition, we demonstrate the generalizability of MPT to 3D hand reconstruction, achieving state-of-the-art results on *FreiHAND* dataset.

1. Introduction

The goal of single-image 3D human pose and mesh reconstruction [14, 16, 27, 29–31, 34–36, 44, 63] is to estimate the 3D coordinates of human body joints and mesh vertices from a single image. Such reconstruction provides key information for human-centric event understanding and motion analysis applications. However, it is challenging due to complex human body articulations, occlusions, and depth ambiguities.

In Computer Vision and Natural Language Processing, the pretrain-and-finetune paradigm [8, 17, 32, 53, 54] has been commonly adopted for performance improvement on

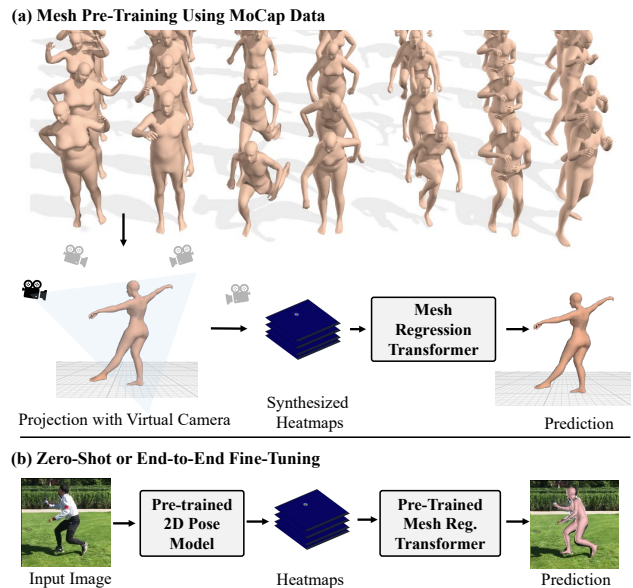


Figure 1. Summary of our pretrain-and-finetune paradigm. (a) Our proposed Mesh Pre-Training (MPT) learns human pose and shape knowledge from large-scale MoCap data without requiring RGB images. (b) After pre-training, our pre-trained model is capable of zero-shot testing on real images, and end-to-end fine-tuning on downstream datasets.

various downstream tasks. For example, researchers [8, 10, 53, 72] propose collecting large-scale image-text pairs from the Internet, and using such large datasets to pre-train transformer models to learn robust representations with cross-modality alignment. The pre-trained models are then fine-tuned for various downstream tasks, achieving significant performance improvements.

Recent studies [14, 35, 36] have also developed transformer models for the task of 3D human pose and mesh reconstruction. The transformer models are effective at capturing the non-local interactions among mesh vertices and body joints for performance improvement. However, researchers [14, 27, 28, 30, 31, 34, 44] typically use image-mesh pairs to train the models in a supervised way to learn

the mapping between 2D images and 3D meshes. When it comes to large-scale pre-training, however, it is non-trivial to scale up the training due to the difficulty of collecting large amounts of image-mesh pairs [57, 63].

In this paper, we present Mesh Pre-Training (MPT), a simple yet effective pre-training method with transformers for human pose and mesh reconstruction from a single image. Different from the existing literature that use image-mesh pairs as training data [14, 27, 30, 31, 34, 44], we explore how to leverage human motion capture (MoCap) data for pre-training. Our idea is motivated by the large amount of MoCap data [40], which provide accurate 3D joint coordinates along with the body mesh. Even though such data cannot be used for end-to-end training due to the lack of RGB images, the data can be used to pre-train the mesh regression transformer subnetwork. For each mesh sample, we select a number of virtual cameras and obtain the 2D coordinates of the joints for each virtual camera. From the 2D joint coordinates, we synthesize heatmaps which are used as the input to the mesh regression transformer subnetwork. We call this pre-training scheme Mesh Pre-Training (MPT). Our MPT model is pre-trained on a large-scale MoCap dataset consisting of 2 million meshes. After the pre-training, the model is fine-tuned and evaluated on the downstream tasks of single-image 3D human pose and mesh reconstruction.

Experimental results show that the proposed MPT advances the state-of-the-art performance on multiple public benchmarks, including Human3.6M [13] and 3DPW [69] datasets. We further show that the proposed MPT enables zero-shot capability, which reconstructs reasonable 3D human meshes on real images without any fine-tuning. In addition, we demonstrate the flexibility of MPT by applying it to the task of single-image 3D hand reconstruction, achieving state-of-the-art results on FreiHAND dataset [78].

In summary, we make the following contributions.

- We introduce Mesh Pre-Training (MPT) that leverages large scale MoCap data to pre-train the mesh regression transformer for the 3D pose and mesh reconstruction from single images.
- We propose to use heatmaps as the intermediate representation to bridge the 2D pose prediction network and the mesh regression transformer, which enables end-to-end fine-tuning.
- The proposed method achieves new state-of-the-art performance on multiple benchmarks including Human3.6M, 3DPW, and FreiHAND.
- MPT enables zero-shot capability of 3D human pose and mesh reconstruction from single images.

2. Related Works

Single-image human pose and mesh reconstruction:

Prior works can be clustered into two categories: parametric and non-parametric approaches. Parametric approaches [20, 27, 28, 30, 33, 51, 67] typically adopt the SMPL model [39] and regress SMPL parameters to generate human meshes. While SMPL model has shown great success and is convenient and robust to pose variations, it is challenging to estimate accurate SMPL parameters from a single image. Thus, researchers [21, 45, 50, 67, 75] have been exploring various auxiliary supervisions such as improving 2D re-projection [34] or extending it to video-based methods [15, 28, 70] to improve the estimation of SMPL parameters.

Different from adopting SMPL as the regression target, non-parametric approaches [14, 16, 31, 35, 36, 44] aim to predict the 3D coordinates of body joints and mesh vertices directly from the input image. Researchers have explored graph convolutional neural networks [16, 31] as well as transformer architecture [14, 35, 36] which is effective in modeling vertex-vertex and vertex-joint interactions for improving the reconstruction performance.

Among the previous works, Pose2Mesh [16] is most relevant to our work. It explores the use of mesh-pose pairs in training. Pose2Mesh shows encouraging results by lifting a 2D poses to a 3D pose, and then generating a 3D mesh based on the 3D pose. They mainly focus on fine-tuning the cascaded graph convolutional neural networks with the pre-specified mesh topology. Our work differs from theirs in multiple aspects. First, we use MoCap data for pre-training while there is no pre-training in their work and they directly add MoCap data to their target dataset for task-specific training. Second, our 2D-pose-to-3D-mesh regression transformer takes heatmaps as input instead of 2D pose coordinates as in Pose2Mesh. The advantage of using heatmaps is that it enables end-to-end training when finetuning for downstream tasks. Third, Pose2Mesh’s 2D-pose-to-3D-mesh regression consists of two separate training steps: 2D-pose-to-3D-pose and 3D-pose-to-3D-mesh while our 2D-pose-to-3D-mesh regression is end-to-end. As we will show in our experiments, our method outperforms Pose2Mesh by a large margin on all the benchmarks.

Synthetic training data generation: Pioneer studies have explored 3D graphics rendering approaches [4, 6, 56, 68] to generate large amount of image-mesh pairs. However, due to the domain gap between real and synthetic images, the trained models usually require domain adaptation techniques [19, 64, 65] to work well on real images. Recent studies [26, 34, 43] also tried to train a human mesh annotator for generating 3D pseudo labels on the real images. Unlike existing works that focused on collecting image-mesh pairs, we propose to use 3D mesh data without RGB images in a pre-training scheme. Our method avoids the require-

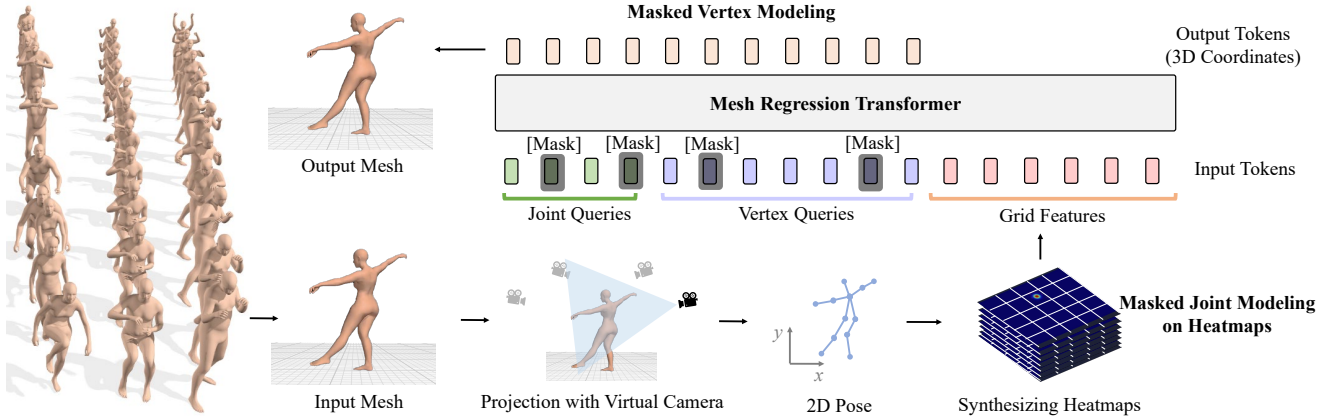


Figure 2. Overview of the proposed Mesh Pre-Training (MPT). Given a human mesh which is sampled from MoCap data, we project its 3D human pose to 2D by randomly selecting a virtual camera. We then synthesize the heatmaps to represent the projected 2D human pose. Our mesh regression transformer takes three types of input tokens, including joint queries, vertex queries, and heatmaps. We then pre-train the transformer to predict the 3D coordinates of body joints and mesh vertices given the input tokens. During pre-training, we perform Masked Joint Modeling and Masked Vertex Modeling to improve the robustness of the mesh regression transformer.

ment for the photorealism of the synthetic data generation, and provides an effective mechanism to leverage 3D mesh datasets that do not have associated RGB images.

Human motion capture (MoCap) datasets: There are many optical marker-based motion capture data available [2, 41, 46, 66], including CMU [1], and AMASS [40]. MoCap data records a variety of human body movements, which is useful for human motion generation and analysis [28, 52, 61, 62]. Since MoCap data is usually captured by the infrared (IR) sensors and performers have to wear special cloth and markers, there are usually no RGB images available. To deal with the problem, prior works [4, 56, 68] proposed to leverage 3D graphics engines to synthesize RGB images for the collection of image-mesh pairs. More recently, researchers have proposed to train a motion discriminator [28] to help improve video-based human mesh reconstruction. Different from prior works, we use MoCap datasets to pre-train our mesh regression subnetwork which improves the accuracy of 3D pose and mesh reconstruction from a single image.

3. Method

Our approach uses a two-stage training scheme that consists of (i) mesh pre-training and (ii) fine-tuning or zero-shot. Figure 1 illustrates our approach using an example. First, in the pre-training stage (Figure 1(a)), the mesh regression transformer learns human mesh reconstruction from heatmaps. This stage uses 3D mesh data without RGB images. The heatmaps are synthesized from 2D joint coordinates which are obtained by projecting 3D joints with a randomly selected virtual camera. Second, Figure 1(b) shows the zero-shot testing on real images. We use an off-the-shelf pre-trained 2D pose estimation model and remove

the post processing operations (which computes 2D coordinates from the heatmaps). The remaining network, which outputs joint heatmaps from an input image, is used as our heatmap regression network. In this way, by plugging in an off-the-shelf pre-trained 2D pose estimation model, our proposed framework performs 3D human pose and mesh reconstruction from an input image. The proposed scheme, for the first time, enables zero-shot reconstruction capability with transformers. Moreover, if the image-mesh pairs are available for a downstream task, we can further fine-tune our model in an end-to-end manner.

There are two reasons why we use heatmaps instead of 2D joint coordinates as the intermediate representation (*i.e.*, the input to the mesh regression transformer). First, using heatmaps enables end-to-end finetuning for downstream tasks. A 2D pose estimation network typically predicts heatmaps first [7, 11, 48, 58, 71, 73]. After that, some non-differentiable post-processing operations such as non-maximum suppression are used to obtain 2D joint coordinates from the heatmaps. Thus it is difficult to perform end-to-end finetuning if we use 2D joint coordinates as the intermediate representation. Second, the conversion from heatmaps to 2D coordinates may cause information loss resulting in suboptimal performance. As we will show later in our experiments (Table 3b), using heatmaps as the intermediate representation outperforms 2D joint coordinates by a large margin in zero-shot setting.

Next, we describe the details of pre-training, zero-shot testing, and fine-tuning.

3.1. Mesh Pre-Training with MoCap Data

As shown in Figure 2, our mesh regression transformer takes three types of tokens as inputs, including joint queries,

vertex queries, and heatmaps. The mesh regression transformer is asked to directly regress the 3D coordinates of body joints and mesh vertices from heatmaps.

We pre-train our mesh regression transformer using a large scale MoCap dataset (*e.g.*, AMASS dataset [40]). Unlike existing works that rely on image-mesh pairs, the proposed Mesh Pre-Training (MPT) is conducted by using 3D mesh data without RGB images. As AMASS dataset consists of sequences of SMPL human meshes, we sparsely sample the human meshes from each motion capture sequence, and then obtain the corresponding 3D human poses using SMPL regressor. This results in a total of 2 million meshes. Note that all the meshes are normalized and centered at the origin. We pre-define 4 virtual cameras above the head positions of the human meshes. For each mesh and each virtual camera, we obtain the projected 2D joint coordinates which are then used to synthesize the joint heatmaps. In this way, we generate 8 million heatmap-mesh pairs which are used in pre-training. More details on the heatmap generation are discussed next.

3.1.1 Synthesizing Heatmaps

Given a mesh, we first project the 3D pose to 2D by randomly selecting a virtual camera. We then represent the 2D pose in the form of heatmaps [12, 58, 71] (also called confidence maps [7]). To be specific, we generate a set of heatmaps \mathbf{S} based on the projected 2D pose. The set $\mathbf{S} = (\mathbf{S}_1, \mathbf{S}_2, \dots, \mathbf{S}_K)$ has K heatmaps, one per joint, where K is the total number of body joints, $\mathbf{S}_j \in \mathbb{R}^{w \times h}$ for $j \in \{1, 2, \dots, K\}$. We set $K = 17$ in our experiments following the body joint definition in COCO dataset [37]. Each heatmap depicts the 2D position of a specified body joint. Let x_j be the 2D coordinate of the body joint j . The value at location \mathbf{p} in the heatmap \mathbf{S}_j is

$$\mathbf{S}_j(\mathbf{p}) = \exp\left(-\frac{\|\mathbf{p} - x_j\|_2^2}{\sigma^2}\right), \quad (1)$$

where $\sigma = 3$ following the literature [58].

In order to input the heatmaps to the transformer model, we concatenate the heatmaps \mathbf{S} along the channel dimension to form a 3D tensor, which is of size $(W \times H \times C)$, and $W = H = 224$. Similar to ViT [18], we split the tensor into non-overlapping patches using a patch partition module [18, 38]. Each patch is then treated as an input token (or grid feature [25]) to the transformer model. In our implementation, we use a patch size of (8×8) . That is, the feature dimension of each patch is $(8 \times 8 \times C)$. Finally, we apply a multi-layer perceptron (MLP) layer to make the dimension of grid features consistent with the hidden size of the transformer model.

3.1.2 Masked Joint Modeling with Heatmaps

During pre-training, we randomly mask some of the joints in the synthesized heatmaps, and ask the mesh regression transformer to predict all the 3D body joints and mesh vertices. Unlike existing works [35, 36] that only used Masked Vertex Modeling to randomly mask out some of the query tokens, we perform masking on the heatmaps. Our masking mechanism is in spirit similar to simulating the real heatmaps obtained from the off-the-shelf 2D pose estimation model, where some joints might be missing. In addition to the masking, we also apply data augmentation to the heatmaps, including adding Gaussian noise and joint jittering.

3.1.3 Pre-Training Objective

Our pre-training objective is a regression task conditioned on the heatmaps. To regress the mesh vertices, following the literature [14, 31, 35, 36], we use L_1 loss to minimize the differences between the predicted vertices V_{3D} and the ground truth vertices \bar{V}_{3D} :

$$\mathcal{L}_V = \frac{1}{M} \sum_{i=1}^M \|V_{3D} - \bar{V}_{3D}\|_1, \quad (2)$$

where $\bar{V}_{3D} \in \mathbb{R}^{M \times 3}$, and M is the total number of vertices.

In addition, we minimize the differences between the predicted joints J_{3D} and the ground truth joints \bar{J}_{3D} :

$$\mathcal{L}_J = \frac{1}{K} \sum_{i=1}^K \|J_{3D} - \bar{J}_{3D}\|_1, \quad (3)$$

where K is the total number of 3D joints.

Note that the 3D joints can be regressed from the mesh vertices using a pre-defined matrix G [14, 16, 27, 30, 31, 34]. We also apply supervision on the regressed 3D joints:

$$\mathcal{L}_J^{reg} = \frac{1}{K} \sum_{i=1}^K \|J_{3D}^{reg} - \bar{J}_{3D}\|_1, \quad (4)$$

where $J_{3D}^{reg} = GV_{3D}$, and $G \in \mathbb{R}^{K \times M}$.

Following the common practice [14, 27, 30, 31, 34–36], we also employ the 2D re-projection loss. Given the predicted 3D joints, we project the predicted 3D joints to 2D using the estimated camera parameters. We then minimize the errors between the projected 2D joints J_{2D} and the ground truth 2D joints \bar{J}_{2D} :

$$\mathcal{L}_J^{proj} = \frac{1}{K} \sum_{i=1}^K \|J_{2D} - \bar{J}_{2D}\|_1. \quad (5)$$

Finally, our pre-training objective can be written as

$$\mathcal{L}_{\text{pre-train}} = \mathcal{L}_V + \mathcal{L}_J + \mathcal{L}_J^{reg} + \mathcal{L}_J^{proj}. \quad (6)$$

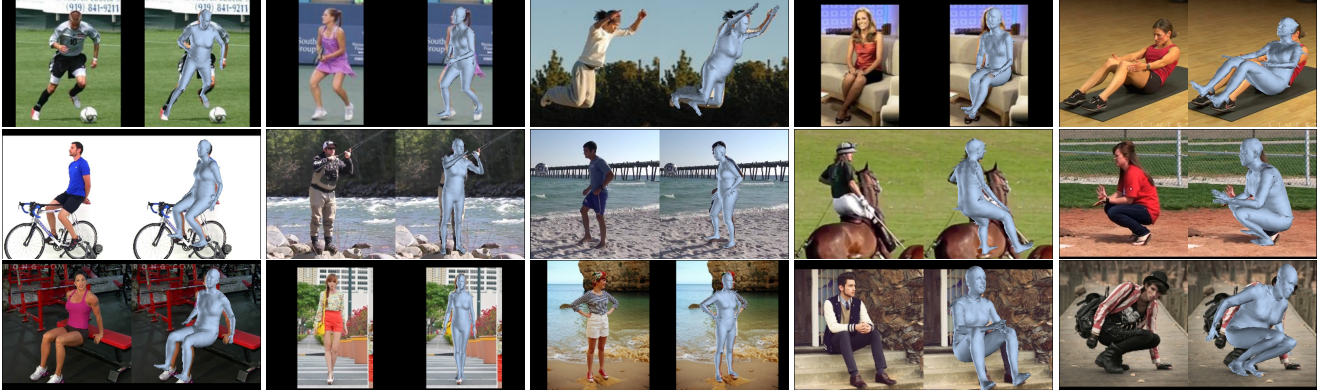


Figure 3. Qualitative examples of our zero-shot reconstruction. MPT generates human meshes on real images in a zero-shot setting.

3.2. Zero-Shot Testing

After pre-training, the pre-trained MPT model can be applied to any real images for zero-shot reconstruction. Given an input image, we use an off-the-shelf 2D pose estimation model to predict the heatmaps. A 2D pose estimation model typically predicts a set of heatmaps first (one heatmap per joint), followed by a series of postprocessing operations to obtain the 2D joint coordinates. We remove those post-processing operations. The remaining network is used as our heatmap regression network to predict heatmaps from a given image.

We then input the predicted heatmaps to the mesh regression transformer for 3D human pose and mesh reconstruction. In this way, our pre-trained MPT model is capable of zero-shot reconstruction in a plug-and-play fashion. It is worth noting that there are many well-performing pre-trained 2D pose estimation models [7, 11, 12, 23, 47, 48, 58, 71, 73] available. In our experiments, we use HigherHRNet [12] as the off-the-shelf 2D pose estimation network.

3.3. End-to-End Fine-Tuning

After pre-training, the pre-trained MPT model can be fine-tuned to the target dataset for more accurate reconstruction. Given the image-mesh pairs from the target dataset, we fine-tune both the heatmap regression network and mesh regression transformer in an end-to-end manner. Similar to our zero-shot experiments, we adopt HigherHRNet [12] as our heatmap regression network.

Our fine-tuning objective is similar to our pre-training. We additionally add an intermediate supervision on top of the heatmap regression network. We follow the existing works [12, 71] and calculate the mean squared error \mathcal{L}_S between the predicted heatmaps \mathbf{S} and the ground truth heatmaps $\hat{\mathbf{S}}$. That is, our fine-tuning objective can be written as

$$\mathcal{L}_{\text{fine-tune}} = \mathcal{L}_V + \mathcal{L}_J + \mathcal{L}_J^{\text{reg}} + \mathcal{L}_J^{\text{proj}} + \mathcal{L}_S. \quad (7)$$

Similar to the existing studies [14, 27, 30, 31, 34–36, 44], we fine-tune our model using a mixture of 2D and 3D datasets. We calculate the losses as long as the ground truths are available.

3.4. Implementation Details

Our mesh regression transformer is in spirit similar to METRO [35]. It consists of multiple transformer layers to regress the 3D coordinates of mesh vertices and body joints. An important difference of our model is that we take heatmaps as input to the transformer network. Heatmaps provide an effective intermediate representation bridging the 2D pose estimation network and mesh regression transformer.

4. Experimental Results

In this section, we first discuss the datasets we used in pre-training and fine-tuning. We then present the performance comparison with existing state-of-the-arts on public benchmarks. Finally, we provide a detailed ablation study to verify the effectiveness of the proposed training scheme.

4.1. Datasets and Evaluation Metrics

We conduct pre-training on AMASS collection [40], which consists of 24 MoCap datasets. AMASS provides a unified human pose and mesh representations based on SMPL [39]. Each sequence records a motion movement of a subject. In total, there are 500 subjects with 17,916 motions. The total length of all the sequences is about 3,772 minutes. In total, there are about 25,088,088 frames, and each frame has a human mesh. To avoid the redundancy between the neighbor frames, we sparsely sample 2 million meshes from AMASS. After projection using 4 virtual cameras, we obtain 8 million heatmap-mesh pairs for pre-training.

We fine-tune our model using a mixture of 2D and 3D datasets, including Human3.6M [24], MuCo-3DHP [42],

Method	3DPW			Human3.6M	
	MPVE ↓	MPJPE ↓	PA-MPJPE ↓	MPJPE ↓	PA-MPJPE ↓
HMR [27]	—	—	81.3	88.0	56.8
GraphCMR [31]	—	—	70.2	—	50.1
SPIN [30]	116.4	96.9	59.2	62.5	41.1
Pose2Mesh [16]	—	89.2	58.9	64.9	47.0
I2LMeshNet [44]	—	93.2	57.7	55.7	41.1
PyMAF [76]	110.1	92.8	58.9	57.7	40.5
ROMP [59]	103.1	85.5	53.3	—	—
VIBE [28]	99.1	82.0	51.9	65.6	41.4
METRO [35]	88.2	77.1	47.9	54.0	36.7
THUNDER [74]	88.0	74.8	51.5	48.0	34.9
PARE [29]	88.6	74.5	46.5	—	—
Graphormer [36]	87.7	74.7	45.6	51.2	34.5
FastMETRO [14]	84.1	73.5	44.6	52.2	33.7
CLIFF [34]	81.2	69.0	43.0	47.1	32.7
MPT (Ours)	79.4	65.9	42.8	45.3	31.7

Table 1. Performance comparison with the previous state-of-the-art methods on 3DPW and Human3.6M datasets.

UP-3D [33], COCO [37], and MPII [3]. Note that these datasets are commonly used in literature [14, 16, 35, 36]. After that, we evaluate our model on Human3.6M using P2 protocol [27, 30]. When conducting experiments on 3DPW [69], we follow the prior works [14, 28, 35, 36] and fine-tune with 3DPW training data. We then evaluate the results on 3DPW test set.

Following literature [14, 27, 30, 31, 34], we use three standard metrics for evaluation, including Mean Per Joint Position Error (MPJPE) [24], Procrustes Analysis with MPJPE (PA-MPJPE) [77], and Mean Per Vertex Error (MPVE) [51]. The unit of the metrics is millimeter (mm).

4.2. Main Results

We compare our method with the existing state-of-the-art approaches on Human3.6M [24] and 3DPW [69] datasets. We present our pretrain-then-finetune results in Table 1. Our method outperforms the previous works on both datasets, including the recent transformer-based methods [14, 35, 36, 74].

It is worth noting that, CLIFF [34] was the state-of-the-art approach on the two datasets. CLIFF additionally leverages the camera focal length and bounding box information to calculate 2D re-projection loss on the non-cropped input image. In contrast, we do not have such post-processing, and still achieve better results, especially on MPJPE.

4.3. Analysis

Effectiveness of Mesh Pre-Training: In our first analysis, we study whether our pre-training is useful for performance improvements. We conduct experiments on Human3.6M, and Table 2 shows the comparison with different training configurations including with or without mesh pre-training, and different datasets for fine-tuning. Because our

Method	MPT	FT	MPJPE ↓	PA-MPJPE ↓
HMR [27]	✗	Mixed Datasets	88.0	56.8
METRO [35]	✗	Mixed Datasets	54.0	36.7
MPT (Ours)	✗	Human3.6M	59.1	39.2
MPT (Ours)	✗	Mixed Datasets	46.6	32.4
MPT (Ours, Zero-shot)	✓	✗	89.0	58.4
MPT (Ours)	✓	Human3.6M	53.3	35.5
MPT (Ours)	✓	Mixed Datasets	45.3	31.7

Table 2. Pre-training analysis. We conduct training with different configurations, and then evaluate results on Human3.6M validation set. MPT: Mesh Pre-Training. FT: Fine-Tuning.

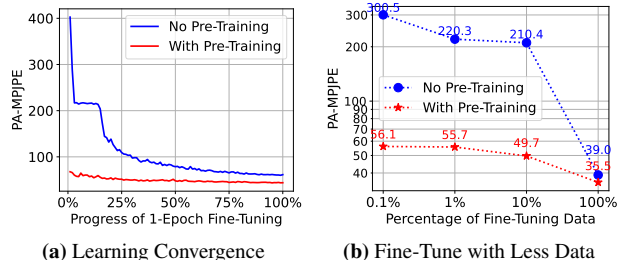


Figure 4. Fine-tuning behavior on Human3.6M. (a) We conduct a 1-epoch fine-tuning and report PA-MPJPE for each fine-tuning step. (b) We use a percentage of Human3.6M data for fine-tuning and report PA-MPJPE.

model architecture is similar to METRO [35], we include it as the reference. We also include the well-known HMR [27] as reference.

In Table 2, our MPT improves the performance across different training configurations considered. When fine-tuning our pre-trained model using Human3.6M only, as shown in the sixth row, MPT achieves 35.5 PA-MPJPE, which is better than 39.2 PA-MPJPE of our non-pretrain model. We observe similar findings when using multiple datasets for fine-tuning. Our MPT achieves 31.5 PA-MPJPE, and is better than 32.4 PA-MPJPE of our non-pretrain model.

Zero-Shot Performance: Given the pre-trained MPT model, we directly test it on real images without any fine-tuning. As shown in the fifth row of Table 2, we obtain a zero-shot performance of 58.4 PA-MPJPE. Although it lags behind the supervised fully fine-tuned models, our zero-shot performance is comparable to the well-known HMR [27]. Figure 3 shows the qualitative zero-shot results. We see that MPT is capable of generating human meshes on real images in a zero-shot setting.

Learning Convergence: We study the impact of MPT during fine-tuning. We perform a 1-epoch fine-tuning on Human3.6M, and report results for each fine-tuning step.

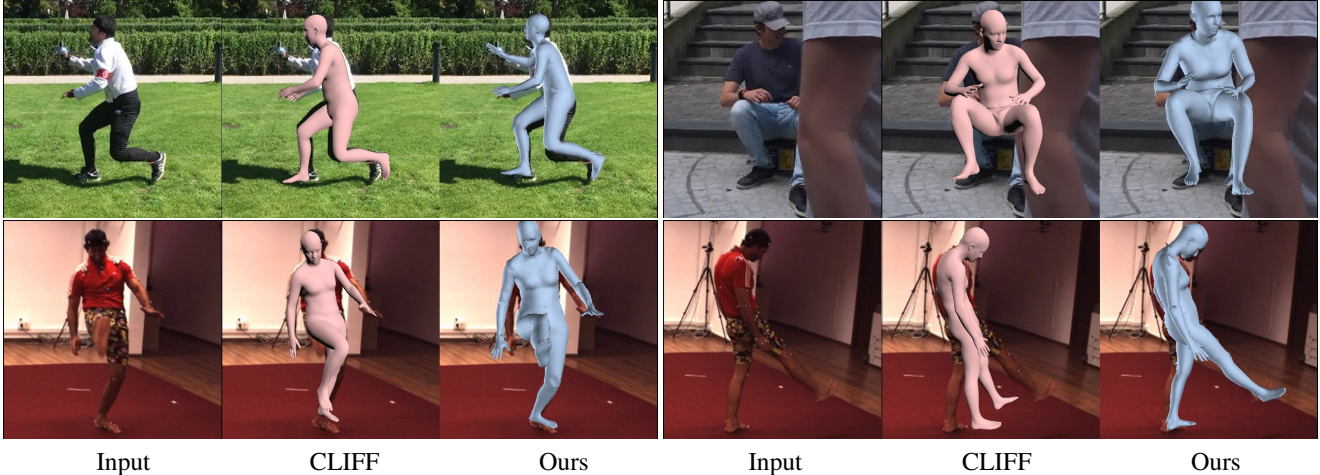


Figure 5. Qualitative comparison. For each example, we show the results from CLIFF [34] and our proposed MPT. Both CLIFF and MPT generate good quality human meshes, but MPT has more favorable body pose. Top row: 3DPW. Bottom row: Human3.6M.

	MPT	MPJPE ↓	PA-MPJPE ↓
Image Features	✗	78.0	47.0
Heatmaps	✗	58.7	39.7
Heatmaps	✓	53.3	35.5

(a) Heatmaps vs. Image Features

	MPJPE ↓	PA-MPJPE ↓
2D Coordinates	139.3	88.9
Heatmaps	88.9	58.4

(b) Heatmaps vs. 2D Coordinates

Method	MPJPE ↓	PA-MPJPE ↓
MPT w/o MJM	97.7	64.4
MPT w/ MJM	88.9	58.4

(c) Masked Joint Modeling with Heatmaps

Table 3. Ablation study of heatmaps: (a) We study different types of grid features, including heatmaps and image features. We conduct end-to-end fine-tuning and evaluation on Human3.6M. (b) Pre-training with different 2D pose representations. We report zero-shot performance on Human3.6M. (c) Ablation study of Masked Joint Modeling for our pre-training. We report zero-shot performance on Human3.6M.

Figure 4a shows that, with our pre-training, the fine-tuning converges better than that without pre-training.

Fine-Tuning with Less Data: We select 0.1%, 1%, and 10% of Human3.6M training data for fine-tuning, respectively. Figure 4b shows that our pre-training helps improve the learning performance when less data is used during fine-tuning. For example, our pre-trained model with 0.1% fine-tune data achieves 56.1 PA-MPJPE, which is much better than 210.4 PA-MPJPE of our non-pretrained model with 10% fine-tune data.

Effectiveness of the Heatmaps: Since we use the heatmaps as the transformer inputs, one may wonder what if we use the image feature maps as discussed in Mesh Graphormer [36]. Clearly we cannot perform mesh pre-training when using image feature maps since there are no RGB images available in mesh pre-training, but one may ask the question that if we only consider end-to-end training (*i.e.*, no mesh pre-training), whether using image feature maps is better than heatmaps. Table 3a shows an ablation study conducted on Human3.6M. We observe that the heatmaps give better results than that of the image feature maps. This shows that heatmaps are more effective inter-

Percentage of PT Data	20%	40%	60%	80%	100%
PA-MPJPE ↓	63.4	62.4	59.9	59.4	58.4

Table 4. Analysis of pre-training data size. We conduct pre-training using different percentage of data, and report zero-shot performance on Human3.6M validation set.

mediate representations than image feature maps.

Comparison between Heatmaps and 2D Coordinates:

A follow-up question is what if we use 2D coordinates instead. We have studied replacing the heatmaps with the 2D coordinates as inputs, and Table 3b shows the zero-shot performance on Human3.6M. We observe that using heatmaps gives better performance. We think this is because heatmaps provide richer information than the 2D coordinates. Note that existing 2D pose estimation networks usually apply a series of post-processing operations (including non-maximum suppression) to the heatmaps for finding the joint locations. Such post-processing may result in information loss.

Ablation Study of Masked Joint Modeling (MJM) on Heatmaps:

Table 3c shows an ablation study of the pro-

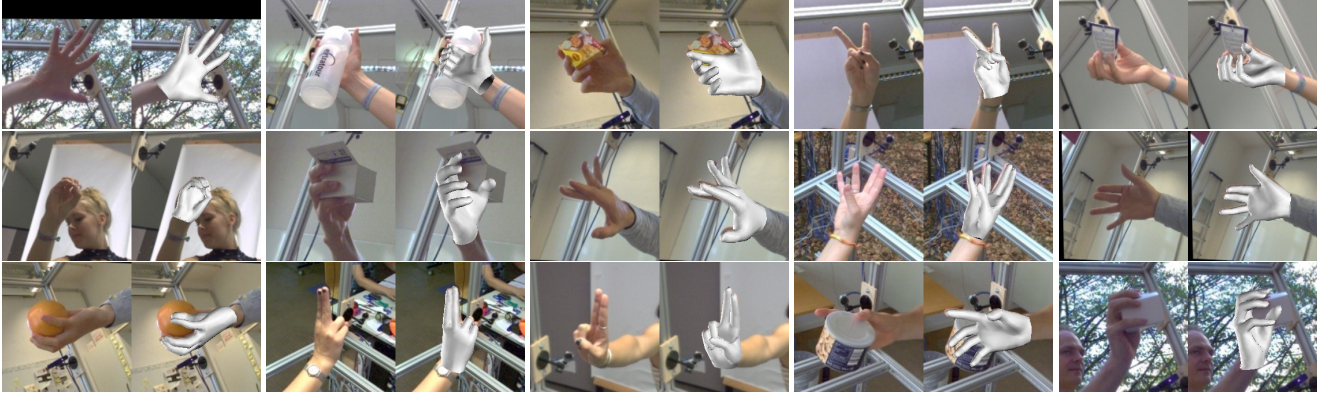


Figure 6. Qualitative results of MPT applying to 3D hand reconstruction on FreiHAND dataset.

Method	PA-MPVPE ↓	PA-MPJPE ↓	F@5 mm ↑	F@15 mm ↑
Hasson et al [22]	13.2	—	0.436	0.908
Boukhayma et al. [5]	13.0	—	0.435	0.898
FreiHAND [78]	10.7	—	0.529	0.935
Pose2Mesh [16]	7.8	7.7	0.674	0.969
I2LMeshNet [44]	7.6	7.4	0.681	0.973
METRO [35]	6.8	6.7	0.717	0.981
Tang et al. [60]	6.7	6.7	0.724	0.981
FastMETRO [14]	—	6.5	—	0.982
Graphormer [36]	6.0	5.9	0.764	0.986
MobRecon [9]	5.7	5.8	0.784	0.986
MPT (Ours)	5.4	5.6	0.789	0.988

Table 5. Performance comparison with the previous state-of-the-art methods on FreiHAND dataset.

Number of Views	1	2	4
PA-MPJPE ↓	61.7	61.4	58.4

Table 6. Ablation study of numbers of virtual camera views. We report zero-shot performance on Human3.6M validation set.

posed Masked Joint Modeling on heatmaps. We observe MJM on heatmaps improves PA-MPJPE by 6 points.

Pre-Training Data Size: Since we use 2 million meshes for pre-training, an interesting question is how much data should we use for pre-training. To answer the question, we conduct pre-training using different percentage of the 2 million meshes. We then report zero-shot performance on Human3.6M validation set. Table 4 shows that increasing the number of meshes for pre-training can improve the zero-shot performance on Human3.6M. The results suggest that we could scale-up our pre-training data for further performance improvements, and we leave it as future work.

Number of Virtual Camera Views: We also study the effect of different number of virtual camera views. Table 6

shows that adding more camera views can improve the zero-shot performance. The results suggest increasing the training data diversity is beneficial to our pre-training.

Qualitative Results: Figure 5 shows the qualitative results of MPT compared with CLIFF [34] on Human3.6M and 3DPW datasets. While both methods can generate good quality human meshes, MPT has more favorable body poses when there are self-occlusions in the images.

Applying to 3D Hand Reconstruction: MPT is a generic pre-training scheme for human mesh regression task. We demonstrate the flexibility of MPT on 3D hand reconstruction, and we conduct the experiments on FreiHAND [78] dataset. Since there is less MoCap data for 3D hands, we use a recently proposed synthetic dataset called Complement [9] for pre-training. Table 5 shows the performance comparison with previous works. MPT outperforms the previous state-of-the-art methods, including MobRecon [9] which also uses Complement as training data. Figure 6 shows the qualitative examples of our hand reconstruction.

5. Conclusion

We introduced Mesh Pre-Training (MPT), a new pre-training framework that leverages large-scale MoCap data to pre-train the mesh regression transformer for 3D human pose and mesh reconstruction from a single image. We propose to use heatmaps as an intermediate representation to bridge the 2D pose estimation model and the mesh regression transformer for end-to-end downstream fine-tuning. Experimental results show that our method advances the state-of-the-art performance on Human3.6M, 3DPW, and FreiHAND datasets. We further show that MPT enables zero-shot reconstruction capability.

References

- [1] Carnegie Mellon University Motion Capture Database. <http://mocap.cs.cmu.edu/>. 3
- [2] Ijaz Akhter and Michael J Black. Pose-conditioned joint angle limits for 3d human pose reconstruction. In *CVPR*, 2015. 3
- [3] Mykhaylo Andriluka, Leonid Pishchulin, Peter Gehler, and Bernt Schiele. 2d human pose estimation: New benchmark and state of the art analysis. In *CVPR*, 2014. 6
- [4] Fabien Baradel, Thibault Groueix, Philippe Weinzaepfel, Romain Brégier, Yannis Kalantidis, and Grégory Rogez. Leveraging mocap data for human mesh recovery. In *3DV*, 2021. 2, 3
- [5] Adnane Boukhayma, Rodrigo de Bem, and Philip HS Torr. 3d hand shape and pose from images in the wild. In *CVPR*, 2019. 8
- [6] Zhongang Cai, Mingyuan Zhang, Jiawei Ren, Chen Wei, Daxuan Ren, Jiatong Li, Zhengyu Lin, Haiyu Zhao, Shuai Yi, Lei Yang, et al. Playing for 3d human recovery. *arXiv preprint arXiv:2110.07588*, 2021. 2
- [7] Zhe Cao, Tomas Simon, Shih-En Wei, and Yaser Sheikh. Realtime multi-person 2d pose estimation using part affinity fields. In *CVPR*, 2017. 3, 4, 5
- [8] Soravit Changpinyo, Piyush Sharma, Nan Ding, and Radu Soricut. Conceptual 12m: Pushing web-scale image-text pre-training to recognize long-tail visual concepts. In *CVPR*, 2021. 1
- [9] Xingyu Chen, Yufeng Liu, Dong Yajiao, Xiong Zhang, Chongyang Ma, Yanmin Xiong, Yuan Zhang, and Xiaoyan Guo. Mobrecon: Mobile-friendly hand mesh reconstruction from monocular image. In *CVPR*, 2022. 8
- [10] Xi Chen, Xiao Wang, Soravit Changpinyo, AJ Piergiovanni, Piotr Padlewski, Daniel Salz, Sebastian Goodman, Adam Grycner, Basil Mustafa, Lucas Beyer, et al. Pali: A jointly-scaled multilingual language-image model. *arXiv preprint arXiv:2209.06794*, 2022. 1
- [11] Yilun Chen, Zhicheng Wang, Yuxiang Peng, Zhiqiang Zhang, Gang Yu, and Jian Sun. Cascaded pyramid network for multi-person pose estimation. In *CVPR*, 2018. 3, 5
- [12] Bowen Cheng, Bin Xiao, Jingdong Wang, Honghui Shi, Thomas S Huang, and Lei Zhang. Higherhrnet: Scale-aware representation learning for bottom-up human pose estimation. In *CVPR*, 2020. 4, 5, 12
- [13] Wei Cheng, Lan Xu, Lei Han, Yuanfang Guo, and Lu Fang. ihuman3d: Intelligent human body 3d reconstruction using a single flying camera. In *ACM MM*, 2018. 2
- [14] Junhyeong Cho, Kim Youwang, and Tae-Hyun Oh. Cross-attention of disentangled modalities for 3d human mesh recovery with transformers. In *ECCV*, 2022. 1, 2, 4, 5, 6, 8
- [15] Hongsuk Choi, Gyeongsik Moon, Ju Yong Chang, and Kyoung Mu Lee. Beyond static features for temporally consistent 3d human pose and shape from a video. In *CVPR*, 2021. 2
- [16] Hongsuk Choi, Gyeongsik Moon, and Kyoung Mu Lee. Pose2mesh: Graph convolutional network for 3d human pose and mesh recovery from a 2d human pose. In *ECCV*, 2020. 1, 2, 4, 6, 8
- [17] Jacob Devlin, Ming-Wei Chang, Kenton Lee, and Kristina Toutanova. Bert: Pre-training of deep bidirectional transformers for language understanding. In *NAACL*, 2019. 1
- [18] Alexey Dosovitskiy, Lucas Beyer, Alexander Kolesnikov, Dirk Weissenborn, Xiaohua Zhai, Thomas Unterthiner, Mostafa Dehghani, Matthias Minderer, Georg Heigold, Sylvain Gelly, et al. An image is worth 16x16 words: Transformers for image recognition at scale. *arXiv preprint arXiv:2010.11929*, 2020. 4
- [19] Salehe Erfanian Ebadi, Saurav Dhakad, Sanjay Vishwakarma, Chunpu Wang, You-Cyuan Jhang, Maciek Chociej, Adam Crespi, Alex Thaman, and Sujoy Ganguly. Psp-hdri +: A synthetic dataset generator for pre-training of human-centric computer vision models. *arXiv preprint arXiv:2207.05025*, 2022. 2
- [20] Peng Guan, Alexander Weiss, Alexandru O Balan, and Michael J Black. Estimating human shape and pose from a single image. In *ICCV*, 2009. 2
- [21] Rıza Alp Güler, Natalia Neverova, and Iasonas Kokkinos. Densepose: Dense human pose estimation in the wild. In *CVPR*, 2018. 2
- [22] Yana Hasson, Gul Varol, Dimitrios Tzionas, Igor Kalevatykh, Michael J Black, Ivan Laptev, and Cordelia Schmid. Learning joint reconstruction of hands and manipulated objects. In *CVPR*, 2019. 8
- [23] Kaiming He, Georgia Gkioxari, Piotr Dollár, and Ross Girshick. Mask r-cnn. In *CVPR*, 2017. 5
- [24] Catalin Ionescu, Dragos Papava, Vlad Olaru, and Cristian Sminchisescu. Human3. 6m: Large scale datasets and predictive methods for 3d human sensing in natural environments. *IEEE Transactions on Pattern Analysis and Machine Intelligence*, 36(7):1325–1339, 2014. 5, 6, 12
- [25] Huaizu Jiang, Ishan Misra, Marcus Rohrbach, Erik Learned-Miller, and Xinlei Chen. In defense of grid features for visual question answering. In *CVPR*, 2020. 4
- [26] Hanbyul Joo, Natalia Neverova, and Andrea Vedaldi. Exemplar fine-tuning for 3d human model fitting towards in-the-wild 3d human pose estimation. In *3DV*, 2021. 2
- [27] Angjoo Kanazawa, Michael J Black, David W Jacobs, and Jitendra Malik. End-to-end recovery of human shape and pose. In *CVPR*, 2018. 1, 2, 4, 5, 6
- [28] Muhammed Kocabas, Nikos Athanasiou, and Michael J. Black. Vibe: Video inference for human body pose and shape estimation. In *CVPR*, 2020. 1, 2, 3, 6
- [29] Muhammed Kocabas, Chun-Hao P Huang, Otmar Hilliges, and Michael J Black. Pare: Part attention regressor for 3d human body estimation. In *ICCV*, 2021. 1, 6
- [30] Nikos Kolotouros, Georgios Pavlakos, Michael J Black, and Kostas Daniilidis. Learning to reconstruct 3d human pose and shape via model-fitting in the loop. In *ICCV*, 2019. 1, 2, 4, 5, 6
- [31] Nikos Kolotouros, Georgios Pavlakos, and Kostas Daniilidis. Convolutional mesh regression for single-image human shape reconstruction. In *CVPR*, 2019. 1, 2, 4, 5, 6, 12
- [32] Alex Krizhevsky, Ilya Sutskever, and Geoffrey E Hinton. Imagenet classification with deep convolutional neural networks. *Communications of the ACM*, 60(6):84–90, 2017. 1

- [33] Christoph Lassner, Javier Romero, Martin Kiefel, Federica Bogo, Michael J Black, and Peter V Gehler. Unite the people: Closing the loop between 3d and 2d human representations. In *CVPR*, 2017. 2, 6
- [34] Zhihao Li, Jianzhuang Liu, Zhensong Zhang, Songcen Xu, and Youliang Yan. Cliff: Carrying location information in full frames into human pose and shape estimation. In *ECCV*, 2022. 1, 2, 4, 5, 6, 7, 8
- [35] Kevin Lin, Lijuan Wang, and Zicheng Liu. End-to-end human pose and mesh reconstruction with transformers. In *CVPR*, 2021. 1, 2, 4, 5, 6, 8, 12
- [36] Kevin Lin, Lijuan Wang, and Zicheng Liu. Mesh graphormer. In *ICCV*, 2021. 1, 2, 4, 5, 6, 7, 8, 12
- [37] Tsung-Yi Lin, Michael Maire, Serge Belongie, James Hays, Pietro Perona, Deva Ramanan, Piotr Dollár, and C Lawrence Zitnick. Microsoft coco: Common objects in context. In *ECCV*, 2014. 4, 6
- [38] Ze Liu, Yutong Lin, Yue Cao, Han Hu, Yixuan Wei, Zheng Zhang, Stephen Lin, and Baining Guo. Swin transformer: Hierarchical vision transformer using shifted windows. In *ICCV*, 2021. 4
- [39] Matthew Loper, Naureen Mahmood, Javier Romero, Gerard Pons-Moll, and Michael J Black. Smpl: A skinned multi-person linear model. *ACM Transactions on Graphics*, 34(6):248, 2015. 2, 5
- [40] Naureen Mahmood, Nima Ghorbani, Nikolaus F Troje, Gerard Pons-Moll, and Michael J Black. Amass: Archive of motion capture as surface shapes. In *ICCV*, 2019. 2, 3, 4, 5, 12
- [41] Christian Mandery, Ömer Terlemez, Martin Do, Nikolaus Vahrenkamp, and Tamim Asfour. The kit whole-body human motion database. In *ICAR*, 2015. 3
- [42] Dushyant Mehta, Oleksandr Sotnychenko, Franziska Mueller, Weipeng Xu, Srinath Sridhar, Gerard Pons-Moll, and Christian Theobalt. Single-shot multi-person 3d pose estimation from monocular rgb. In *3DV*, 2018. 5
- [43] Gyeongsik Moon, Hongsuk Choi, and Kyoung Mu Lee. Neuralannot: Neural annotator for 3d human mesh training sets. In *CVPR Workshop*, 2022. 2
- [44] Gyeongsik Moon and Kyoung Mu Lee. I2l-meshnet: Image-to-lixel prediction network for accurate 3d human pose and mesh estimation from a single rgb image. In *ECCV*, 2020. 1, 2, 5, 6, 8
- [45] Gyeongsik Moon and Kyoung Mu Lee. Pose2pose: 3d positional pose-guided 3d rotational pose prediction for expressive 3d human pose and mesh estimation. *arXiv preprint arXiv:2011.11534*, 2020. 2
- [46] Meinard Müller, Andreas Baak, and Hans-Peter Seidel. Efficient and robust annotation of motion capture data. In *ACM SIGGRAPH/Eurographics Symposium on Computer Animation*, 2009. 3
- [47] Alejandro Newell, Zhiao Huang, and Jia Deng. Associative embedding: End-to-end learning for joint detection and grouping. In *NeurIPS*, 2017. 5
- [48] Alejandro Newell, Kaiyu Yang, and Jia Deng. Stacked hourglass networks for human pose estimation. In *ECCV*, 2016. 3, 5
- [49] Adam Paszke, Sam Gross, Francisco Massa, Adam Lerer, James Bradbury, Gregory Chanan, Trevor Killeen, Zeming Lin, Natalia Gimelshein, Luca Antiga, et al. Pytorch: An imperative style, high-performance deep learning library. *NeurIPS*, 2019. 12
- [50] Georgios Pavlakos, Jitendra Malik, and Angjoo Kanazawa. Human mesh recovery from multiple shots. *arXiv preprint arXiv:2012.09843*, 2020. 2
- [51] Georgios Pavlakos, Luyang Zhu, Xiaowei Zhou, and Kostas Daniilidis. Learning to estimate 3d human pose and shape from a single color image. In *CVPR*, 2018. 2, 6
- [52] Mathis Petrovich, Michael J Black, and Gül Varol. Temos: Generating diverse human motions from textual descriptions. *arXiv preprint arXiv:2204.14109*, 2022. 3
- [53] Alec Radford, Jong Wook Kim, Chris Hallacy, Aditya Ramesh, Gabriel Goh, Sandhini Agarwal, Girish Sastry, Amanda Askell, Pamela Mishkin, Jack Clark, et al. Learning transferable visual models from natural language supervision. In *ICML*, 2021. 1
- [54] Alec Radford, Karthik Narasimhan, Tim Salimans, and Ilya Sutskever. Improving language understanding by generative pre-training. *Technical report*, 2018. 1
- [55] Jeff Rasley, Samyam Rajbhandari, Olatunji Ruwase, and Yuxiong He. Deepspeed: System optimizations enable training deep learning models with over 100 billion parameters. In *KDD*, 2020. 12
- [56] Grégory Rogez and Cordelia Schmid. Mocap-guided data augmentation for 3d pose estimation in the wild. *NeurIPS*, 2016. 2, 3
- [57] Yu Rong, Ziwei Liu, Cheng Li, Kaidi Cao, and Chen Change Loy. Delving deep into hybrid annotations for 3d human recovery in the wild. In *ICCV*, 2019. 2
- [58] Ke Sun, Bin Xiao, Dong Liu, and Jingdong Wang. Deep high-resolution representation learning for human pose estimation. In *CVPR*, 2019. 3, 4, 5
- [59] Yu Sun, Qian Bao, Wu Liu, Yili Fu, Michael J Black, and Tao Mei. Monocular, one-stage, regression of multiple 3d people. In *ICCV*, 2021. 6
- [60] Xiao Tang, Tianyu Wang, and Chi-Wing Fu. Towards accurate alignment in real-time 3d hand-mesh reconstruction. In *ICCV*, 2021. 8
- [61] Guy Tevet, Brian Gordon, Amir Hertz, Amit H Bermano, and Daniel Cohen-Or. Motionclip: Exposing human motion generation to clip space. *arXiv preprint arXiv:2203.08063*, 2022. 3
- [62] Guy Tevet, Sigal Raab, Brian Gordon, Yonatan Shafir, Daniel Cohen-Or, and Amit H Bermano. Human motion diffusion model. *arXiv preprint arXiv:2209.14916*, 2022. 3
- [63] Yating Tian, Hongwen Zhang, Yebin Liu, and Limin Wang. Recovering 3d human mesh from monocular images: A survey. *arXiv preprint arXiv:2203.01923*, 2022. 1, 2
- [64] Josh Tobin, Rachel Fong, Alex Ray, Jonas Schneider, Wojciech Zaremba, and Pieter Abbeel. Domain randomization for transferring deep neural networks from simulation to the real world. In *IROS*, 2017. 2
- [65] Jonathan Tremblay, Aayush Prakash, David Acuna, Mark Brophy, Varun Jampani, Cem Anil, Thang To, Eric Cameracci, Shaad Boochoon, and Stan Birchfield. Training deep

- networks with synthetic data: Bridging the reality gap by domain randomization. In *CVPR Workshop*, 2018. 2
- [66] Nikolaus F Troje. Decomposing biological motion: A framework for analysis and synthesis of human gait patterns. *Journal of vision*, 2(5):2–2, 2002. 3
- [67] Hsiao-Yu Tung, Hsiao-Wei Tung, Ersin Yumer, and Katerina Fragkiadaki. Self-supervised learning of motion capture. In *NeurIPS*, 2017. 2
- [68] Gül Varol, Javier Romero, Xavier Martin, Naureen Mahmood, Michael J. Black, Ivan Laptev, and Cordelia Schmid. Learning from synthetic humans. In *CVPR*, 2017. 2, 3
- [69] Timo von Marcard, Roberto Henschel, Michael Black, Bodo Rosenhahn, and Gerard Pons-Moll. Recovering accurate 3d human pose in the wild using imus and a moving camera. In *ECCV*, 2018. 2, 6
- [70] Ziniu Wan, Zhengjia Li, Maoqing Tian, Jianbo Liu, Shuai Yi, and Hongsheng Li. Encoder-decoder with multi-level attention for 3d human shape and pose estimation. In *ICCV*, 2021. 2
- [71] Jingdong Wang, Ke Sun, Tianheng Cheng, Borui Jiang, Chaorui Deng, Yang Zhao, Dong Liu, Yadong Mu, Mingkui Tan, Xinggang Wang, Wenyu Liu, and Bin Xiao. Deep high-resolution representation learning for visual recognition. *IEEE Transactions on Pattern Analysis and Machine Intelligence*, 2019. 3, 4, 5
- [72] Jianfeng Wang, Zhengyuan Yang, Xiaowei Hu, Linjie Li, Kevin Lin, Zhe Gan, Zicheng Liu, Ce Liu, and Lijuan Wang. Git: A generative image-to-text transformer for vision and language. *arXiv preprint arXiv:2205.14100*, 2022. 1
- [73] Bin Xiao, Haiping Wu, and Yichen Wei. Simple baselines for human pose estimation and tracking. In *ECCV*, 2018. 3, 5
- [74] Mihai Zanfir, Andrei Zanfir, Eduard Gabriel Bazavan, William T Freeman, Rahul Sukthankar, and Cristian Sminchisescu. Thundr: Transformer-based 3d human reconstruction with markers. In *ICCV*, 2021. 6
- [75] Hongwen Zhang, Jie Cao, Guo Lu, Wanli Ouyang, and Zhenan Sun. Learning 3d human shape and pose from dense body parts. *IEEE Trans. Pattern Anal. Mach. Intell.*, 2020. 2
- [76] Hongwen Zhang, Yating Tian, Xinchu Zhou, Wanli Ouyang, Yebin Liu, Limin Wang, and Zhenan Sun. Pymaf: 3d human pose and shape regression with pyramidal mesh alignment feedback loop. In *ICCV*, 2021. 6
- [77] Xiaowei Zhou, Menglong Zhu, Georgios Pavlakos, Spyridon Leonardos, Konstantinos G Derpanis, and Kostas Daniilidis. Monocap: Monocular human motion capture using a cnn coupled with a geometric prior. *IEEE Transactions on Pattern Analysis and Machine Intelligence*, 2018. 6
- [78] Christian Zimmermann, Duygu Ceylan, Jimei Yang, Bryan Russell, Max Argus, and Thomas Brox. Freihand: A dataset for markerless capture of hand pose and shape from single rgb images. In *ICCV*, 2019. 2, 8

Supplementary Material

Number of Views	MPJPE ↓	PA-MPJPE ↓
1	92.5	61.7
2	89.5	61.4
4	89.0	58.4
8	88.3	58.2

Table 7. Adding more virtual camera views. We report zero-shot performance on Human3.6M validation set.

Resolution	MPJPE ↓	PA-MPJPE ↓
112×112	46.5	32.7
224×224	45.3	31.7

Table 8. Different resolutions of the heatmaps. We conduct fine-tuning on a mixture of 2D and 3D training sets, and evaluate the performance on Human3.6M validation set.

A. Details of Virtual Cameras

During pre-training, we use virtual cameras to help synthesize heatmaps. In order to set up the virtual cameras at proper positions, we follow the camera settings of Human3.6M [24] in our experiments. To be specific, we set up 4 virtual cameras using the camera parameters from Subject 1 of Human3.6M training set.

B. Adding More Virtual Cameras

We further investigate whether adding more camera views can improve the performance. Given the 4 virtual cameras defined by Human3.6M, we perform interpolation to obtain additional 4 virtual camera views. Figure 7 illustrates our virtual cameras using an example. The 4 virtual cameras defined by Human3.6M are denoted in black color. The interpolated virtual cameras are denoted in green color.

In Table 7, we observe that adding more camera views in pre-training improves the zero-shot performance for both metrics on Human3.6M.

C. Heatmap Resolution

As we use HigherHRNet [12] to generate high resolution heatmaps, one may wonder what resolution is needed. Table 8 shows the performance comparison with different resolutions. The results suggest that using larger resolution (*i.e.*, 224×224) can slightly improve the results. We note that HigherHRNet was pre-trained using the non-cropped images [12], but we use 224×224 cropped images instead. We think that increasing the input resolution to the original resolution on which HigherHRNet was trained could further enhance model performance.

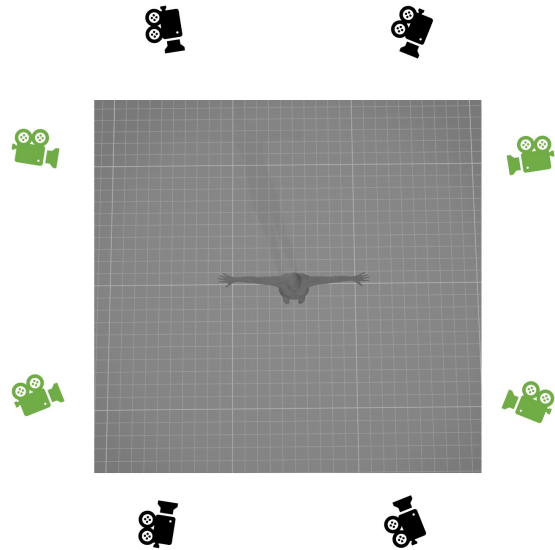


Figure 7. Illustration of our virtual cameras in a top-down view. In order to set up a virtual camera at a proper position, we follow the camera settings of Human3.6M to set up 4 virtual cameras (indicated in black color). In addition, we perform interpolation to obtain extra virtual camera positions (indicated in green color).

D. Additional Implementation Details

We implement our models based on PyTorch [49] and Graphormer codebase [35, 36]. We additionally adopt DeepSpeed [55] which empirically leads to faster and more stable training. We use 16 NVIDIA V100 GPUs for most of our training experiments. We use the Adam optimizer for training. We set the initial learning rate as 2×10^{-4} , and then use learning rate warmup over the first 10% training steps followed by linear decay to 0. We perform mesh pre-training on the 2 million meshes (sparsely sampled from AMASS dataset [40]) for 10 epochs. When fine-tuning on mixed datasets, we empirically fine-tune for 80 epochs.

Our HigherHRNet is with HRNet-w48 architecture initialized with COCO Keypoint pre-trained weights [12]. We use the same transformer architecture as in the literature [35, 36]. Specifically, our transformer model has 3 transformer blocks. Each block has 4 transformer layers and 4 attention heads. For the 3 transformer blocks, the hidden sizes are 1024, 256, 64, respectively. To reduce the computational cost, the transformer model outputs a coarse mesh. We then use MLPs to upsample the predicted mesh to the original resolution, similar to [35, 36]. For simplicity, we do not add graph convolutions to the transformer layers.

Following the literature [31, 36], we use a weak perspective camera model for calculating 2D re-projection loss. Our model predicts camera parameters, including a scaling

factor s and a 2D translation vector t . Our method does not leverage ground truth camera parameters. The camera parameters are learned by optimizing 2D re-projection.

E. Limitations and Societal Impact

3D pose estimation models can be potentially applied to human activity analysis applications, such as detecting whether the senior subjects are falling. However, there is a risk associated with directly applying the models for mission-critical decision making, especially in the health care field. Real-world applications may require an auxiliary supervision model or task-specific fine-tuning.

Our models have a dependency on existing MoCap training data. Some of the public released MoCap data may be licensed, meaning they can only be used for scientific research purposes. Users must strictly adhere to the data usage agreement to utilize MoCap datasets for their intended purposes.